References

1) Duan L, Bao XY, Yang WZ, Shi WC, Li DS, Zhang ZS, Zong R, Han C, Zhao F, Feng J: Moyamoya Disease in China: Its Clinical Features and Outcomes. *Stroke* Oct 20, 2011 Online

2) Goto Y, Yonekawa Y: Worldwide distribution of moyamoya disease. *Neurol Med Chir (Tokyo)* 32: 883-886, 1992

3) Ikezaki K, Han DH, Kawano T, Kinukawa N, Fukui M: A clinical comparison of definite moyamoya disease between South Korea and Japan. *Stroke* 28, 2513-2517, 1997

4) Kamada F, Aoki Y, Narisawa A, Abe Y, Komatsuzaki S, Kikuchi A, Kanno J, Niihori T, Ono M, Ishii N, Owada Y, Fujimura M, Mashimo Y, Suzuki Y, Hata A, Tsuchiya S, Tominaga T, Matsubara Y, Kure S: A genome-wide association study identifies RNF213 as the first Moyamoya disease gene. *J Hum Genet* 56, 34-40, 2011

5) Koizumi A, Harada KH, Inoue K, Hitomi T, Yang HR, Moon CS, Wang P, Hung NN, Watanabe T, Shimbo S, Ikeda M: Past, present, and future of environmental specimen banks. *Environ Health Prev Med* 14, 307-318, 2009

6) Koizumi A, Yoshinaga T, Harada K, Inoue K, Morikawa A, Muroi J, Inoue S, Eslami B, Fujii S, Fujimine Y, Hachiya N, Koda S, Kusaka Y, Murata K, Nakatsuka H, Omae K, Saito N, Shimbo S, Takenaka K, Takeshita T, Todoriki H, Wada Y, Watanabe T, Ikeda M: Assessment of human exposure to polychlorinated biphenyls and polybrominated diphenyl ethers in Japan using archived samples from the early 1980s and mid-1990s. *Environ Res.* 99, 31-39, 2005

7) Kuroda S, Houkin K: Moyamoya disease: current concepts and future perspectives.

Lancet Neurol 7: 1056-1066, 2008

8) Liu W, Hashikata H, Inoue K, Matsuura N, Mineharu Y, Kobayashi H, Kikuta KI, Takagi Y, Hitomi T, Krischek B, Zou LP, Fang F, Herzig R, Kim JE, Kang HS, Oh CW, Tregouet DA, Hashimoto N, Koizumi A: A rare Asian founder polymorphism of Raptor may explain the high prevalence of Moyamoya disease among East Asians and its low prevalence among Caucasians. *Environ Health Prev Med* 15: 94-104, 2010

9) Liu W, Morito D, Takashima S, Mineharu Y, Kobayashi H, Hitomi T, Hashikata H, Matsuura N, Yamazaki S, Toyoda A, Kikuta K, Takagi Y, Harada KH, Fujiyama A, Herzig R, Krischek B, Zou L, Kim JE, Kitakaze M, Miyamoto S, Nagata K, Hashimoto N, Koizumi A: Identification of RNF213 as a susceptibility gene for moyamoya disease and its possible role in vascular development. *PLoS One* 6(7):e22542, 2011

10) Miao W, Zhao PL, Zhang YS, Liu HY, Chang Y, Ma J, Huang QJ, Lou ZX: Epidemiological and clinical features of Moyamoya disease in Nanjing, China. *Clin Neurol Neurosurg* 112: 199-203, 2010

11) Mineharu Y, Liu W, Inoue K, Matsuura N, Inoue S, Takenaka K, Ikeda H, Houkin K, Takagi Y, Kikuta K, Nozaki K, Hashimoto N, Koizumi A: Autosomal dominant moyamoya disease maps to chromosome 17q25.3. *Neurology* 70: 2357-2363, 2008

12) Suzuki J, Takaku A: Cerebrovascular "moyamoya" disease. Disease showing abnormal net-like vessels in base of brain. *Arch Neurol* 20: 288-299, 1969

13) Takeuchi K, Shimizu K: Hypogenesis of bilateral internal carotid arteries. *Brain Nerve* 9: 37-43, 1957

Figure legend

Figure 1. Locations of the sampling sites in East and Southeast Asian countries.

re 1

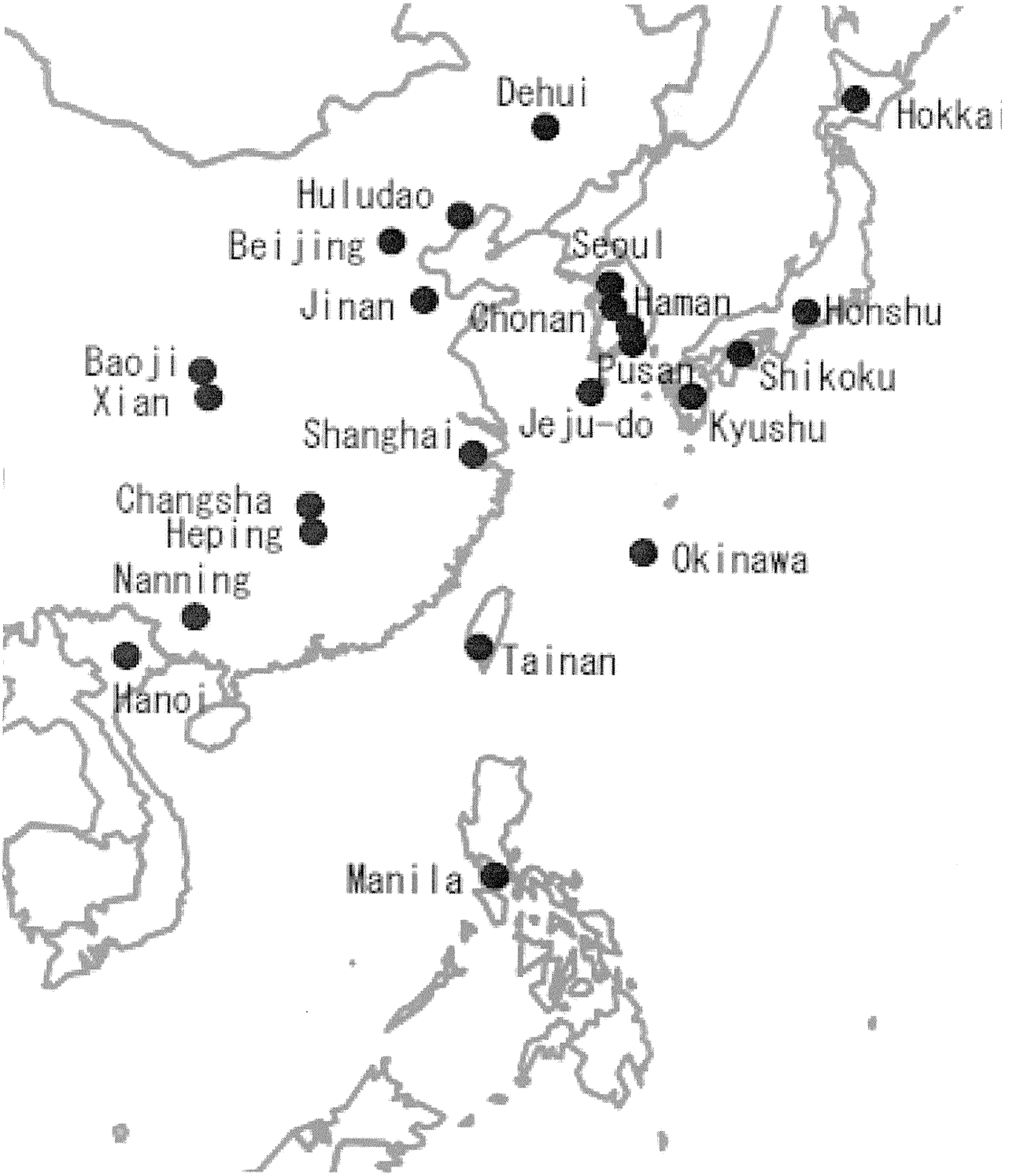
Dehui
Hokkai
Huludao
Beijing
Seoul
Jinan
Chonan
Haman
Honshu
Baoji
Xian
Pusan
Shikoku
Shanghai
Jeju-do
Kyushu
Changsha
Heping
Okinawa
Nanning
Tainan
Hanoi
Manila

Table 1. Demographic features of the participants in the East and Southeast Asian populations.

Area	Country	Location	Size of population (million)	Male: Female	Age (y): mean ± SD	Angiography[a]
East Asia	China	Dehui	1.00	0: 50	NA	0
		Huludao	2.82	0: 50	NA	0
		Beijing	19.61	0: 50	38.4 ± 10.6	0
		Jinan	6.81	0: 50	NA	0
		Xian	8.47	0 : 94	NA	0
		Baoji	3.72	0 : 48	NA	0
		Shanghai	23.02	0: 50	NA	0
		Changsha	7.04	0: 50	NA	0
		Heping	4.60	0: 46	NA	0
		Nanning	6.66	0: 50	NA	0
		Tainan	1.88	0: 49	36.4 ± 11.5	0
		Total	85.63	0: 587	37.4 ± 11.1	0
	Korea	Seoul	10.46	80: 25	42.2 ± 13.3	46
		Chonan	0.58	0: 29	34.6 ± 8.8	0
		Haman	0.06	0: 46	43.6 ± 6.8	0
		Pusan	3.60	0: 49	39.4 ± 7.8	0
		Jeju-do	0.53	0: 65	NA	0
		Total	15.23	80: 214	40.9 ± 10.9	46
	Japan	Mainland	123.62	608: 766	57.7 ± 14.1	384
		Okinawa	1.38	0: 100	47.5 ± 7.2	0
		Total	125.00	608: 866	57.0 ± 14.0	384
Southeast Asia	Vietnam	Hanoi	6.50	0: 103	22.8 ± 10.2	0
	Philippines	Manila	1.66	0: 50	NA	0

SD: standard deviation; NA: not applicable.

[a]Angiography: conventional digital subtraction angiography, magnetic resonance angiography, computed tomography angiography and others.

Table 2. Geographic distribution of p.R4810K in *RNF213* in East and Southeast Asian populations.

Area	Country	Location	Genotype of p.R4810K			Sample size	Minor allele frequency (%)	Total Population (million)	Estimated population with p.R4810K in a country (million)
			GG	GA	AA				
East Asia	China	Dehui	50	0	0	50	0.00	1340.00	11.41
		Huludao	50	0	0	50	0.00		
		Beijing	49	1	0	50	1.00		
		Jinan	50	0	0	50	0.00		
		Xian	92	2	0	94	1.06		
		Baoji	48	0	0	48	0.00		
		Shanghai	49	1	0	50	1.00		
		Changsha	50	0	0	50	0.00		
		Heping	46	0	0	46	0.00		
		Nanning	49	1	0	50	1.00		
		Tainan	49	0	0	49	0.00		
		Total	582	5	0	587	0.43		
	Korea	Seoul	102	3	0	105	1.43	50.00	1.36
		Chonan	28	1	0	29	1.72		
		Haman	45	1	0	46	1.09		
		Pusan	48	1	0	49	1.02		
		Jeju-do	63	2	0	65	1.54		
		Total	286	8	0	294	1.36		
	Japan	Mainland	1339	32	3	1374	1.38	125.00	3.39
		Okinawa	98	2	0	100	1.00		
		Total	1437	34	3	1474	1.36		
Southeast Asia	Vietnam	Hanoi	103	0	0	103	0.00	90.50	0.00
	Philippines	Manila	50	0	0	50	0.00	94.00	0.00

Expansion of Intronic GGCCTG Hexanucleotide Repeat in *NOP56* Causes SCA36, a Type of Spinocerebellar Ataxia Accompanied by Motor Neuron Involvement

Hatasu Kobayashi,[1,4] Koji Abe,[2,4] Tohru Matsuura,[2,4] Yoshio Ikeda,[2] Toshiaki Hitomi,[1] Yuji Akechi,[2] Toshiyuki Habu,[3] Wanyang Liu,[1] Hiroko Okuda,[1] and Akio Koizumi[1,*]

Autosomal-dominant spinocerebellar ataxias (SCAs) are a heterogeneous group of neurodegenerative disorders. In this study, we performed genetic analysis of a unique form of SCA (SCA36) that is accompanied by motor neuron involvement. Genome-wide linkage analysis and subsequent fine mapping for three unrelated Japanese families in a cohort of SCA cases, in whom molecular diagnosis had never been performed, mapped the disease locus to the region of a 1.8 Mb stretch (LOD score of 4.60) on 20p13 (D20S906–D20S193) harboring 37 genes with definitive open reading frames. We sequenced 33 of these and observed a large expansion of an intronic GGCCTG hexanucleotide repeat in *NOP56* and an unregistered missense variant (Phe265Leu) in *C20orf194*, but we found no mutations in *PDYN* and *TGM6*. The expansion showed complete segregation with the SCA phenotype in family studies, whereas Phe265Leu in *C20orf194* did not. Screening of the expansions in the SCA cohort cases revealed four additional occurrences, but none were revealed in the cohort of 27 Alzheimer disease cases, 154 amyotrophic lateral sclerosis cases, or 300 controls. In total, nine unrelated cases were found in 251 cohort SCA patients (3.6%). A founder haplotype was confirmed in these cases. RNA foci formation was detected in lymphoblastoid cells from affected subjects by fluorescence in situ hybridization. Double staining and gel-shift assay showed that (GGCCUG)n binds the RNA-binding protein SRSF2 but that $(CUG)_6$ does not. In addition, transcription of *MIR1292*, a neighboring miRNA, was significantly decreased in lymphoblastoid cells of SCA patients. Our finding suggests that SCA36 is caused by hexanucleotide repeat expansions through RNA gain of function.

Autosomal-dominant spinocerebellar ataxias (SCAs) are a heterogeneous group of neurodegenerative disorders characterized by loss of balance, progressive gait, and limb ataxia.[1–3] We recently encountered two unrelated patients with intriguing clinical symptoms from a community in the Chugoku region in western mainland Japan.[4] These patients both showed complicated clinical features, with ataxia as the first symptom, followed by characteristic late-onset involvement of the motor neuron system that caused symptoms similar to those of amyotrophic lateral sclerosis (ALS [MIM 105400]).[4] Some SCAs (SCA1 [MIM 164400], SCA2 [MIM 183090], SCA3 [MIM 607047], and SCA6 [MIM 183086]) are known to slightly affect motor neurons; however, their involvement is minimal and the patients usually do not develop skeletal muscle and tongue atrophies.[4] Of particular interest is that RNA foci have been recently demonstrated in hereditary disorders caused by microsatellite repeat expansions or insertions in the noncoding regions of their gene.[5–7] The unique clinical features in these families have seldom been described in previous reports; therefore, we undertook a genetic analysis.

A similar form of SCA was observed in five Japanese cases from a cohort of 251 patients with SCA, in whom molecular diagnosis had not been performed, who were followed by the Department of Neurology, Okayama University Hospital. These five cases originated from a city of 450,000 people in the Chugoku region. Thus, we suspected the presence of a founder mutation common to these five cases, prompting us to recruit these five families (pedigrees 1–5) (Figure 1, Table 1). This study was approved by the Ethics Committee of Kyoto University and the Okayama University institutional review board. Written informed consent was obtained from all subjects. An index of cases per family was investigated in some depth: IV-4 in pedigree 1, II-1 in pedigree 2, III-1 in pedigree 3, II-1 in pedigree 4, and II-1 in pedigree 5. The mean age at onset of cerebellar ataxia was 52.8 ± 4.3 years, and the disease was transmitted by an autosomal-dominant mode of inheritance. All affected individuals started their ataxic symptoms, such as gait and truncal instability, ataxic dysarthria, and uncoordinated limbs, in their late forties to fifties. MRI revealed relatively confined and mild cerebellar atrophy (Figure 2A). Unlike individuals with previously known SCAs, all affected individuals with longer disease duration showed obvious signs of motor neuron involvement (Table 1). Characteristically, all affected individuals exhibited tongue atrophy with fasciculation, although its degree of severity varied (Figure 2B). Despite severe tongue atrophy in some cases, their swallowing function was relatively preserved, and they were allowed oral intake even at a later point after onset. In addition to tongue atrophy, skeletal muscle atrophy and fasciculation in the limbs and trunk appeared in advanced cases.[4] Tendon reflexes were generally mildly to severely hyperreactive in most

[1]Department of Health and Environmental Sciences, Graduate School of Medicine, Kyoto University, Kyoto, Japan; [2]Department of Neurology, Graduate School of Medicine, Dentistry and Pharmaceutical Science, Okayama University, Okayama, Japan; [3]Radiation Biology Center, Kyoto University, Kyoto, Japan
[4]These authors contributed equally to this work
*Correspondence: koizumi.akio.5v@kyoto-u.ac.jp
DOI 10.1016/j.ajhg.2011.05.015.

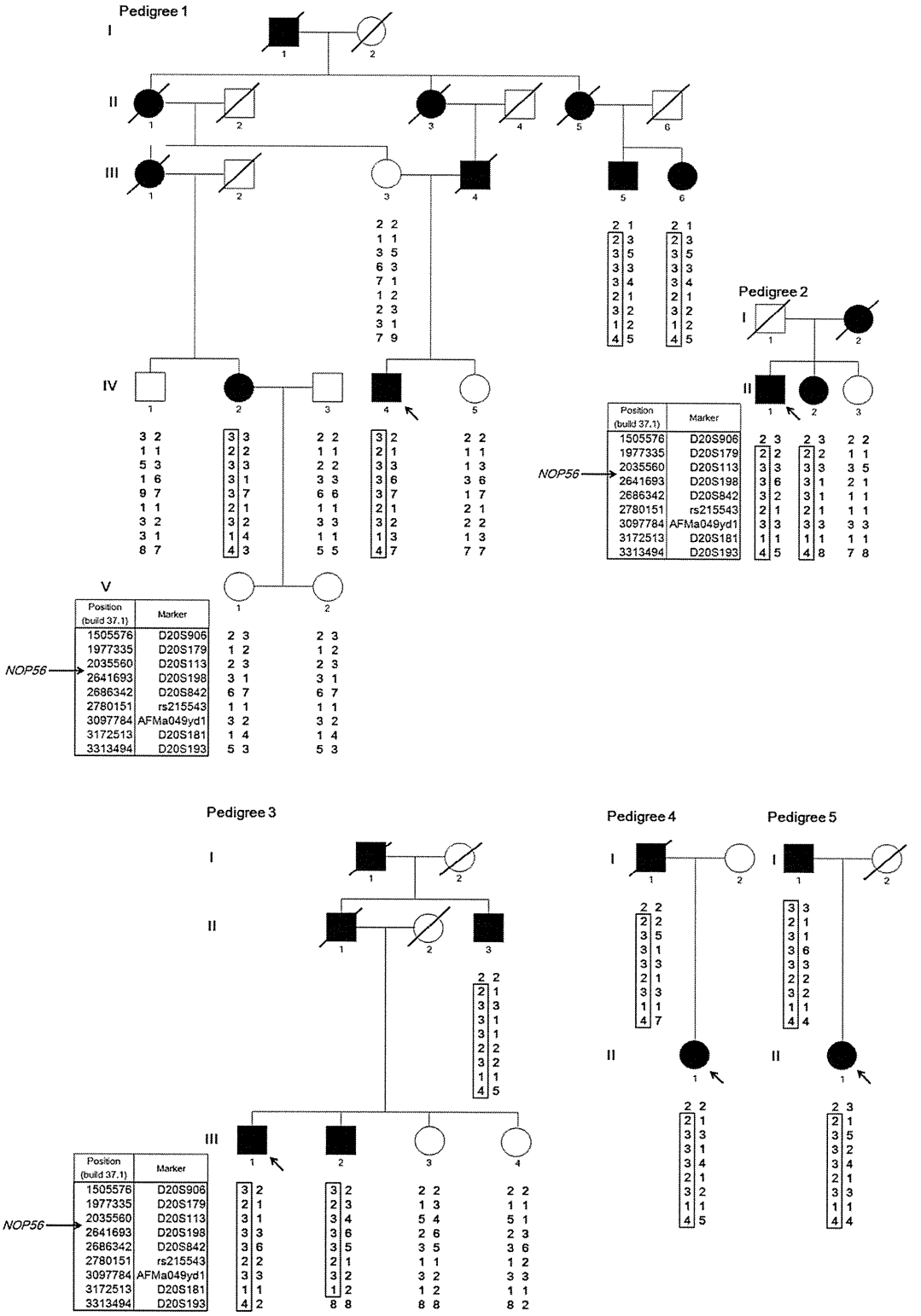

Figure 1. Pedigree Charts of the Five SCA Families
Haplotypes are shown for nine markers from D20S906 (1,505,576 bp) to D20S193 (3,313,494 bp), spanning 1.8 Mb on chromosome 20p13. *NOP56* is located at 2,633,254–2,639,039 bp (NCBI build 37.1). Filled and unfilled symbols indicate affected and unaffected individuals, respectively. Squares and circles represent males and females, respectively. A slash indicates a deceased individual. The putative founder haplotypes among patients are shown in boxes constructed by GENHUNTER.[8] Arrows indicate the index case. The pedigrees were slightly modified for privacy protection.

Table 1. Clinical Characteristics of Affected Subjects

Pedigree No.	Patient ID	Gender	Onset Age (yr)	Current Age (yr)	Ataxia	Motor Neuron Involvement			Genotype of GGCCTG Repeats
						Skeletal Muscle Atrophy	Skeletal Muscle Fasciculation	Tongue Atrophy/ Fasciculation	
1	III-5	M	50	70	+++	N.D.	N.D.	N.D.	g.263397_263402[6]+(1800)
	III-6	F	52	68	++	+	+	+	g.263397_263402[6]+(2300)
	IV-2	F	57	63	+	-	-	+	g.263397_263402[6]+(2300)
	IV-4	M	50	59	+	-	-	+	g.263397_263402[6]+(2300)
2	II-1	M	55	77	+++	++	+	+	g.263397_263402[6]+(2200)
	II-2	F	53	70	++	N.D.	N.D.	N.D.	g.263397_263402[6]+(2200)
3	II-3	M	58	77	++	++	+	+	g.263397_263402[3]+(2300)
	III-1	M	56	62	+	-	-	±	g.263397_263402[8]+(2200)
	III-2	M	51	61	++	+	+	+	g.263397_263402[6]+(1800)
4	I-1	M	57	died in 2001 at 83	++	N.D.	N.D.	N.D.	g.263397_263402[5]+(1800)
	II-1	F	48	61	++	+	±	++	g.263397_263402[6]+(2000)
5	I-1	M	57	86	++	+++	+	+	g.263397_263402[5]+(2000)
	II-1	F	47	58	++	+	+	+	g.263397_263402[8]+(1700)
	SCA#1	M	52	69	+++	+++	+++	+++	g.263397_263402[5]+(2200)
	SCA#2	F	43	53	+++	-	-	+	g.263397_263402[6]+(1800)
	SCA#3	M	55	60	++	-	-	++	g.263397_263402[8]+(1700)
	SCA#4	M	57	81	+++	+	+	+++	g.263397_263402[5]+(2200)
Mean			52.8						
SD			4.3						

N.D., not determined.

affected individuals, none of whom displayed severe lower limb spasticity or extensor plantar response. Electrophysiological studies were performed in an affected individual. Nerve conduction studies revealed normal findings in all of the cases that were examined; however, an electromyogram showed neurogenic changes only in cases with skeletal muscle atrophy, indicating that lower motor neuropathy existed in this particular disease. Progression of motor neuron involvement in this SCA was typically limited to the tongue and main proximal skeletal muscles in both upper and lower extremities, which is clearly different from typical ALS, which usually involves most skeletal muscles over the course of a few years, leading to fatal results within several years.

We conducted genome-wide linkage analysis for nine affected subjects and eight unaffected subjects in three informative families (pedigrees 1–3; Figure 1). For genotyping, we used an ABI Prism Linkage Mapping Set (Version 2; Applied Biosystems, Foster City, CA, USA) with 382 markers, 10 cM apart, for 22 autosomes. Fine-mapping markers (approximately 1 cM apart) were designed according to information from the uniSTS reference physical map in the NCBI database. A parametric linkage analysis was carried out in GENEHUNTER[8] with the assumption of an autosomal-dominant model. The disease allele frequency was set at 0.000001, and a phenocopy frequency of 0.000001 was assumed. Population allele frequencies were assigned equal portions of individual alleles. We performed multipoint analyses for autosomes and obtained LOD scores. We considered LOD scores above 3.0 to be significant.[8] Genome-wide linkage analysis revealed a single locus on chromosome 20p13 with a LOD score of 3.20. Fine mapping increased the LOD score to 4.60 (Figure 3). Haplotype analysis revealed two recombination events in pedigree 3, delimiting a1.8 Mb region (D20S906–D20S193) (Figure 1). We further tested whether the five cases shared the haplotype. As shown in Figure 1, pedigrees 4 and 5 were confirmed to have the same haplotype as pedigrees 1, 2, and 3, indicating that the 1.8 Mb region is very likely to be derived from a common ancestor.

The 1.8 Mb region harbors 44 genes (NCBI, build 37.1). We eliminated two pseudogenes and five genes (*LOC441938*, *LOC100289473*, *LOC100288797*, *LOC100289507*, and *LOC100289538*) from the candidates. Evidence view showed that the first, fourth, and fifth genes were not found in the contig in this region, whereas the second and third

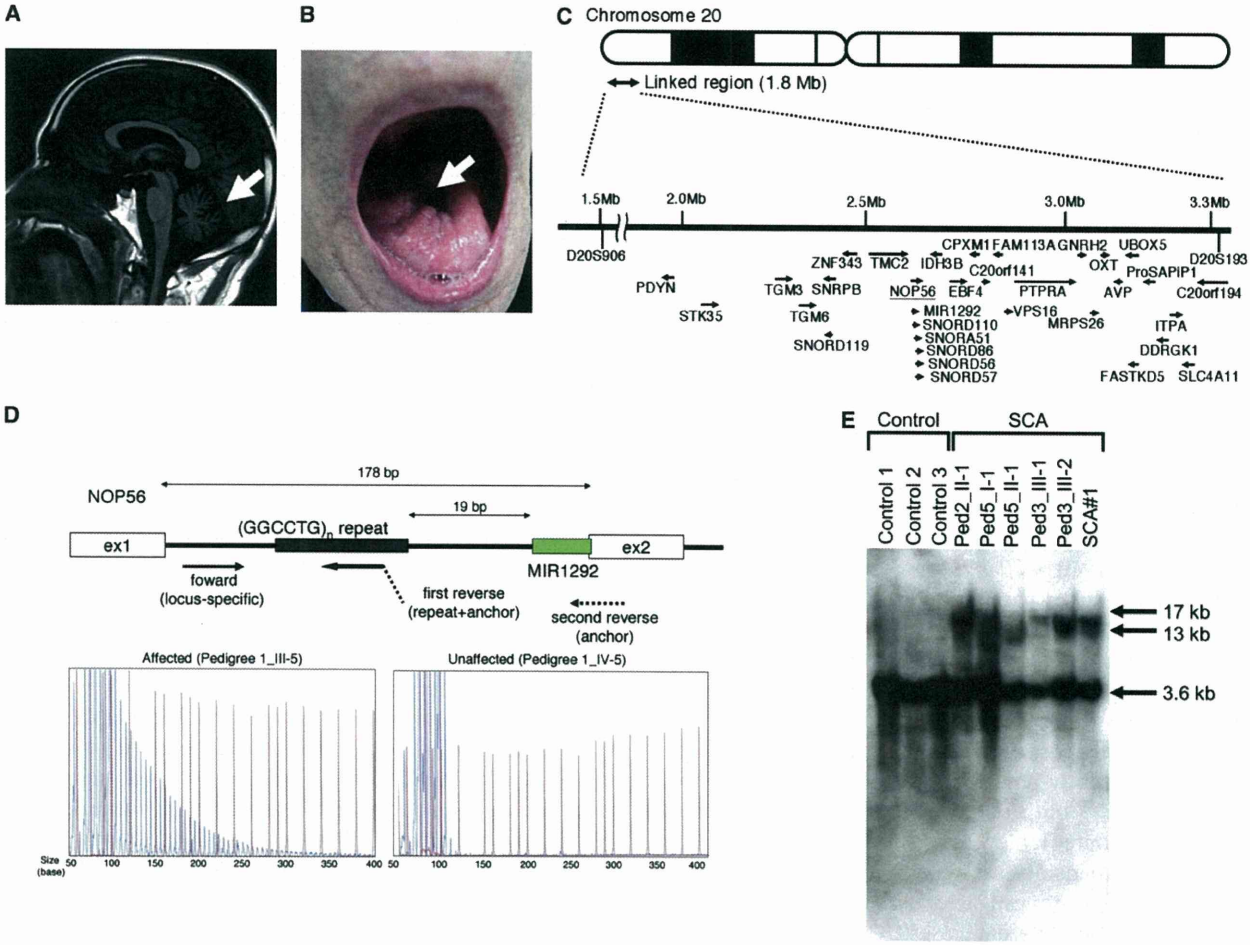

Figure 2. Motor Neuron Involvement and (GGCCTG)n Expansion in the First Intron of *NOP56*
(A) MRI of an affected subject (SCA#3) showed mild cerebellar atrophy (arrow) but no other cerebral or brainstem pathology.
(B) Tongue atrophy (arrow) was observed in SCA#1.
(C) Physical map of the 1.8-Mb linkage region from D20S906 (1,505,576 bp) to D20S193 (3,313,494 bp), with 33 candidate genes shown, as well as the direction of transcription (arrows).
(D) The upper portion of the panel shows the scheme of primer binding for repeat-primer PCR analysis. In the lower portion, sequence traces of the PCR reactions are shown. Red lines indicate the size markers. The vertical axis indicates arbitrary intensity levels. A typical saw-tooth pattern is observed in an affected pedigree.
(E) Southern blotting of LCLs from SCA cases and three controls. Genomic DNA (10 μg) was extracted from Epstein-Barr virus (EBV)-immortalized LCLs derived from six affected subjects (Ped2_II-1, Ped3_III-1, Ped3_III-2, Ped5_I-1, Ped5_II-1, and SCA#1) and digested with 2 U of *AvrII* overnight (New England Biolabs, Beverly, MA, USA). A probe covering exon 4 of *NOP56* (452 bp) was subjected to PCR amplification from human genomic DNA with the use of primers (Table S3) and labeled with ^{32}P-dCTP.

genes are not assigned to orthologous loci in the mouse genome. Sequence similarities among paralog genes defied direct sequencing of four genes: *SIRPD* [NM 178460.2], *SIRPB1* [NM 603889], *SIRPG* [NM 605466], and *SIRPA* [NM 602461]. Thus, we sequenced 33 of 37 genes (*PDYN* [MIM 131340], *STK35* [MIM 609370], *TGM3* [MIM 600238], *TGM6* [NM_198994.2], *SNRPB* [MIM 182282], *SNORD119* [NR_003684.1], *ZNF343* [NM_024325.4], *TMC2* [MIM 606707], *NOP56* [NM_006392.2], *MIR1292* [NR_031699.1], *SNORD110* [NR_003078.1], *SNORA51* [NR_002981.1], *SNORD86* [NR_004399.1], *SNORD56* [NR_002739.1], *SNORD57* [NR_002738.1], *IDH3B* [MIM 604526], *EBF4* [MIM 609935], *CPXM1* [NM_019609.4], *C20orf141* [NM_080739.2], *FAM113A* [NM_022760.3], *VPS16* [MIM 608550], *PTPRA* [MIM 176884], *GNRH2* [MIM 602352], *MRPS26* [MIM 611988], *OXT* [MIM 167050], *AVP* [MIM 192340], *UBOX5* [NM_014948.2], *FASTKD5* [NM_021826.4], *ProSAPiP1* [MIM 610484], *DDRGK1* [NM_023935.1], *ITPA* [MIM 147520], *SLC4A11* [MIM 610206], and *C20orf194* [NM_001009984.1]) (Figure 2C). All noncoding and coding exons, as well as the 100 bp up- and downstream of the splice junctions of these genes, were sequenced in two index cases (IV-4 in pedigree1 and III-1 in pedigree 3) and in three additional cases (II-1 in pedigree 2, II-1 in pedigree 4, and II-1 in pedigree 5) with the use of specific primers (Table S1 available online). Eight unregistered variants were found among the two index cases. Among these, there was a coding variant, c.795C>G

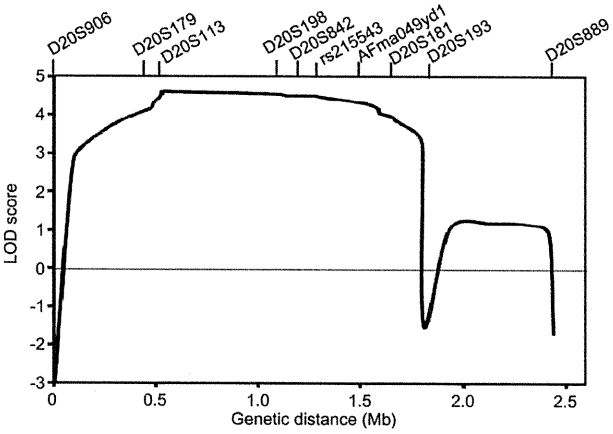

Figure 3. Multipoint Linkage Analysis with Ten Markers on Chromosome 20p13

(p.Phe265Leu), in *C20orf194*, whereas the other seven included one synonymous variant, c.1695T>A (p.Leu565-Leu), in *ZNF343* and six non-splice-site intronic variants (Table S2). We tested segregation by sequencing exon 11 of *C20orf194* in IV-2 and III-5 in pedigree 1. Neither IV-2 nor III-5 had this variant. We thus eliminated *C20orf194* as a candidate. Missense mutations in *PDYN* and *TGM6*, which have been recently reported as causes of SCA, mapped to 20p12.3-p13,[9,10] but none were detected in the five index cases studied here (Table S2).

Possible expansions of repetitive sequences in these 33 genes were investigated when intragenic repeats were indicated in the database (UCSC Genome Bioinformatics). Expansions of the hexanucleotide repeat GGCCTG (rs68063608) were found in intron 1 of *NOP56* (Figure 2D) in all five index cases through the use of a repeat-primed PCR method.[11–13] An outline of the repeat-primed PCR experiment is described in Figure 2D. In brief, the fluorescent-dye-conjugated forward primer corresponded to the region upstream of the repeat of interest. The first reverse primer consisted of four units of the repeat (GGCCTG) and a 5′ tail used as an anchor. The second reverse primer was an "anchor" primer. These primers are described in Table S3. Complete segregation of the expanded hexanucleotide was confirmed in all pedigrees, and the maximum repeat size in nine unaffected members was eight (data not shown).

In addition to the SCA cases in five pedigrees, four unrelated cases (SCA#1–SCA#4) were found to have a (GGCCTG)n allele through screening of the cohort SCA patients (Table 1). Neurological examination was reevaluated in these four cases, revealing both ataxia and motor neuron dysfunction with tongue atrophy and fasciculation (Table 1). In total, nine unrelated cases were found in the 251 cohort patients with SCA (3.6%). For confirmation of the repeat expansions, Southern blot analysis was conducted in six affected subjects (Ped2_II-1, Ped3_III-1, Ped3_III-2, Ped5_I-1, Ped5_II-1, and SCA#1). The data showed >10 kb of repeat expansions in the lymphoblastoid cell lines (LCLs) obtained from the SCA patients (Figure 2E). Furthermore, the numbers of GGCCTG repeat expansion were estimated by Southern blotting in 11 other cases. The expansion analysis revealed approximately 1500 to 2500 repeats in 17 cases (Table 1). There was no negative association between age at onset and the number of GGCCTG repeats ($n = 17$, $r = 0.42$, $p = 0.09$; Figure S1) and no obvious anticipation in the current pedigrees.

To investigate the disease specificity and disease spectrum of the hexanucleotide repeat expansions, we tested the repeat expansions in an Alzheimer disease (MIM 104300) cohort and an ALS cohort followed by the Department of Neurology, Okayama University Hospital. We also recruited Japanese controls, who were confirmed to be free from brain lesions through MRI and magnetic resonance angiography, which was performed as described previously.[14] Screening of the 27 Alzheimer disease cases and 154 ALS cases failed to detect additional cases with repeat expansions. The GGCCTG repeat sizes ranged from 3 to 8 in 300 Japanese controls (5.9 ± 0.8 repeats), suggesting that the >10 kb repeat expansions were mutations.

Expression of *Nop56*, an essential component of the splicing machinery,[15] was examined by RT-PCR with the use of primers for wild-type mouse *Nop56* cDNA (Table S3). Expression of *Nop56* mRNA was detected in various tissues, including CNS tissue, and a very weak signal was detected in spinal cord tissue (Figure 4A). Immunohistochemistry using an anti-mouse Nop56 antibody (Santa Cruz Biotechnology, Santa Cruz, CA, USA) detected the Nop56 protein in Purkinje cells of the cerebellum as well as motor neurons of the hypoglossal nucleus and the spinal cord anterior horn (Figure 4B), suggesting that these cells may be responsible for tongue and muscle atrophy in the trunk and limbs, respectively. Immunoblotting also confirmed the presence of Nop56 in neural tissues (Figure 4C), where Nop56 is localized in both the nucleus and cytoplasm.

Alterations of *NOP56* RNA expression and protein levels in LCLs from patients were examined by real-time RT-PCR and immunoblotting. The primers for quantitative PCR of human *NOP56* cDNA are described in Table S3. Immunoblotting was performed with the use of an anti-human NOP56 antibody (Santa Cruz Biotechnology, Santa Cruz, CA, USA). We found no decrease in *NOP56* RNA expression or protein levels in LCLs from these patients (Figure 5A). To investigate abnormal splicing variants of *NOP56*, we performed RT-PCR using the primers covering the region from the 5′ UTR to exon 4 around the repeat expansion (Table S3); however, no splicing variant was observed in LCLs from the cases (Figure 5B). We also performed immunocytochemistry for NOP56 and coilin, a marker of the Cajal body, where NOP56 functions.[16] NOP56 and coilin distributions were not altered in LCLs of the SCA patients (Figure 5C), suggesting that qualitative or quantitative changes in the Cajal body did not occur. These results indicated that haploinsufficiency could not explain the observed phenotype.

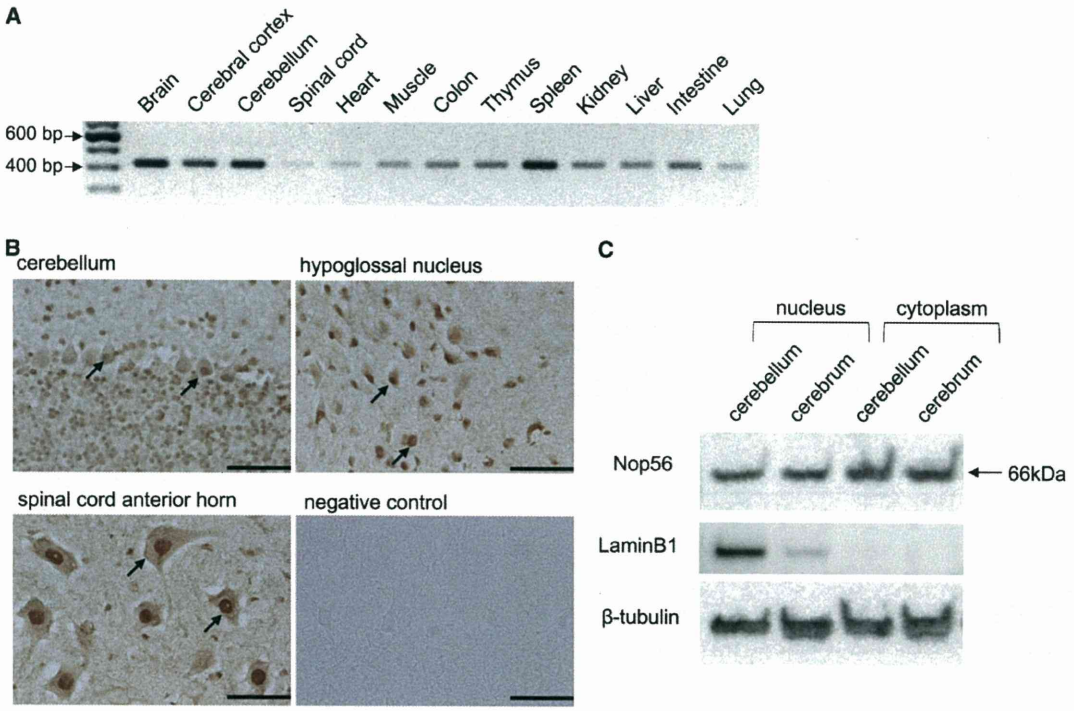

Figure 4. Nop56 in the Mouse Nervous System
(A) RT-PCR analysis of Nop56 (422 bp) in various mouse tissues. cDNA (25 ng) collected from various organs of C57BL/6 mice was purchased from GenoStaf (Tokyo, Japan).
(B) Immunohistochemical analysis of Nop56 in the cerebellum, hypoglossal nucleus, and spinal cord anterior horn in wild-type male Slc:ICR mice at 8 wks of age (Japan SLC, Shizuoka, Japan). The arrows indicate anti- Nop56 antibody staining. The negative control was the cerebellar sample without the Nop56 antibody treatment. Scale bar represents 100 μm.
(C) Immunoblotting of Nop56 (66 kDa) in the cerebellum and cerebrum. Protein sample (10 μg) was subjected to immunoblotting. LaminB1, a nuclear protein, and beta-tubulin were used as loading controls.

We performed fluorescence in situ hybridization to detect RNA foci containing the repeat transcripts in LCLs from patients, as previously described.[17,18] Lymphoblastoid cells from two SCA patients (Ped2_II-2 and Ped5_I-1) and two control subjects were analyzed. An average of 2.1 ± 0.5 RNA foci per cell were detected in 57.0% of LCLs (n = 100) from the SCA subjects through the use of a nuclear probe targeting the GGCCUG repeat, whereas no RNA foci were observed in control LCLs (n = 100) (Figure 6A). In contrast, a probe for the CGCCUG repeat, another repeat sequence in intron 1 of *NOP56*, detected no RNA foci in either SCA or control LCLs (n = 100 each) (Figure 6A), indicating that the GGCCUG repeat was specifically expanded in the SCA subjects. The specificity of the RNA foci was confirmed by sensitivity to RNase A treatment and resistance to DNase treatment (Figure 6A).

Several reports have suggested that RNA foci play a role in the etiology of SCA through sequestration of specific RNA-binding proteins.[5–7] In silico searches (ESEfinder 3.0) predicted an RNA-binding protein, SRSF2 (MIM 600813), as a strong candidate for binding of the GGCCUG repeat. Double staining with the probe for the GGCCUG repeat and an anti-SRSF2 antibody (Sigma-Aldrich, Tokyo, Japan) was performed. The results showed colocalization of RNA foci with SRSF2, whereas NOP56 and coilin were not colocalized with the RNA foci (Figure 6B), suggesting a specific interaction of endogenous SRSF2 with the RNA foci in vivo.

To further confirm the interaction, gel-shift assays were carried out for investigation of the binding activity of SRSF2 with $(GGCCUG)_n$. Synthetic RNA oligonucleotides (200 pmol), $(GGCCUG)_4$ or $(CUG)_6$, which is the latter part of the hexanucleotide, as well as the repeat RNA involved in myotonic dystrophy type 1 (DM1 [MIM 160900])[18] and SCA8 (MIM 608768),[5] were denatured and immediately mixed with different amounts (0, 0.2, or 0.6 μg) of recombinant full-length human SRSF2 (Abcam, Cambridge, UK). The mixtures were incubated, and the protein-bound probes were separated from the free forms by electrophoresis on 5%–20% native polyacrylamide gels. The separated RNA probes were detected with SYBR Gold staining (Invitrogen, Carlsbad, CA, USA). We found a strong association of $(GGCCUG)_4$ with SRSF2 in vitro in comparison to $(CUG)_6$ (Figure 6C). Collectively, we concluded that (GGCCUG)n interacts with SRSF2.

It is notable that *MIR1292* is located just 19 bp 3′ of the GGCCTG repeat (Figure 2D). MiRNAs such as *MIR1292* are small noncoding RNAs that regulate gene expression by inhibiting translation of specific target mRNAs.[19,20] MiRNAs are believed to play important roles in key molecular

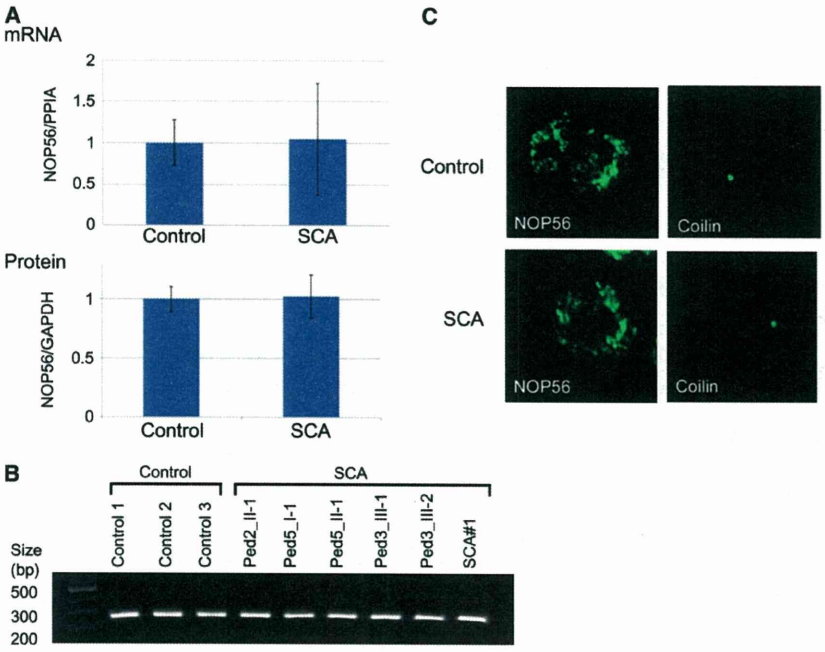

Figure 5. Analysis of NOP56 in LCLs from SCA Patients

(A) mRNA expression (upper panel) and protein levels (lower panel) in LCLs from cases (n = 6) and controls (n = 3) were measured by RT-PCR and immunoblotting, respectively. cDNA (10 ng) was transcribed from total RNA isolated from LCLs and used for RT-PCR. Immunoblotting was performed with the use of a protein sample (40 μg) extracted from LCLs. The data indicate the mean ± SD relative to the levels of *PP1A* and GAPDH, respectively. There was no significant difference between LCLs from controls and cases.

(B) Analysis for splicing variants of NOP56 cDNA. RT-PCR with 10 ng of cDNA and primers corresponding to the region from the 5′ UTR to exon 4 around the repeat expansion was performed. The PCR product has an expected size of 230 bp.

(C) Immunocytochemistry for NOP56 and coilin. Green signals represent NOP56 or coilin. Shown are representative samples from 100 observations of controls or cases.

pathways by fine-tuning gene expression.[19,20] Recent studies have revealed that miRNAs influence neuronal survival and are also associated with neurodegenerative diseases.[21,22] In silico searches (Target Scan Human 5.1) predicted glutamate receptors (*GRIN2B* [MIM 138252] and *GRIK3* [MIM 138243]) to be potential target genes. Real-time RT-PCR using TaqMan probes for miRNA (Invitrogen, Carlsbad, CA, USA) revealed that the levels of both mature and precursor *MIR1292* were significantly decreased in SCA LCLs (Figure 6D), indicating that the GGCCTG repeat expansion decreased the transcription of *MIR1292*. A decrease in *MIR1292* expression may upregulate glutamate receptors in particular cell types; e.g., *GRIK3* in stellate cells in the cerebellum,[23] leading to ataxia because of perturbation of signal transduction to the Purkinje cells. In addition, it has been suggested, on the basis of ALS mouse models,[24,25] that excitotoxicity mediated by a type of glutamate receptor, the NMDA receptor including *GRIN2B*, is involved in loss of spinal neurons. A very slowly progressing and mild form of the motor neuron disease, such as that described here, which is limited to mostly fasciculation of the tongue, limbs and trunk, may also be compatible with such a functional dysregulation rather than degeneration.

In the present study, we have conducted genetic analysis to find a genetic cause for the unique SCA with motor neuron disease. With extensive sequencing of the 1.8 Mb linked region, we found large hexanucleotide repeat expansions in *NOP56,* which were completely segregated with SCA in five pedigrees and were found in four unrelated cases with a similar phenotype. The expansion was not found in 300 controls or in other neurodegenerative diseases. We further proved that repeat expansions of *NOP56* induce RNA foci and sequester SRSF2. We thus concluded that hexanucleotide repeat expansions are considered to cause SCA by a toxic RNA gain-of-function mechanism, and we name this unique SCA as SCA36. Haplotype analysis indicates that hexanucleotide expansions are derived from a common ancestor. The prevalence of SCA36 was estimated at 3.6% in the SCA cohort in Chugoku district, suggesting that prevalence of SCA36 may be geographically limited to the western part of Japan and is rare even in Japanese SCAs.

Expansion of tandem nucleotide repeats in different regions of respective genes (most often the triplets CAG and CTG) has been shown to cause a number of inherited diseases over the past decades. An expansion in the coding region of a gene causes a gain of toxic function and/or reduces the normal function of the corresponding protein at the protein level. RNA-mediated noncoding repeat expansions have also been identified as causing eight other neuromuscular disorders: DM1, DM2 (MIM 602668), fragile X tremor/ataxia syndrome (FXTAS [MIM 300623]), Huntington disease-like 2 (HDL2 [MIM 606438]), SCA8, SCA10 (MIM 603516), SCA12 (MIM 604326), and SCA31 (MIM 117210).[26] The repeat numbers in affected alleles of SCA36 are among the largest seen in this group of diseases (i.e., there are thousands of repeats). Moreover, SCA36 is not merely a nontriplet repeat expansion disorder similar to SCA10, DM2, and SCA31, but is now proven to be a human disease caused by a large hexanucleotide repeat expansion. In addition, no or only weak anticipation has been reported for noncoding repeat expansion in SCA, whereas clear anticipation has been reported for most polyglutamine expansions in SCA.[2] As such, absence of anticipation in SCA36 is in accord with previous studies

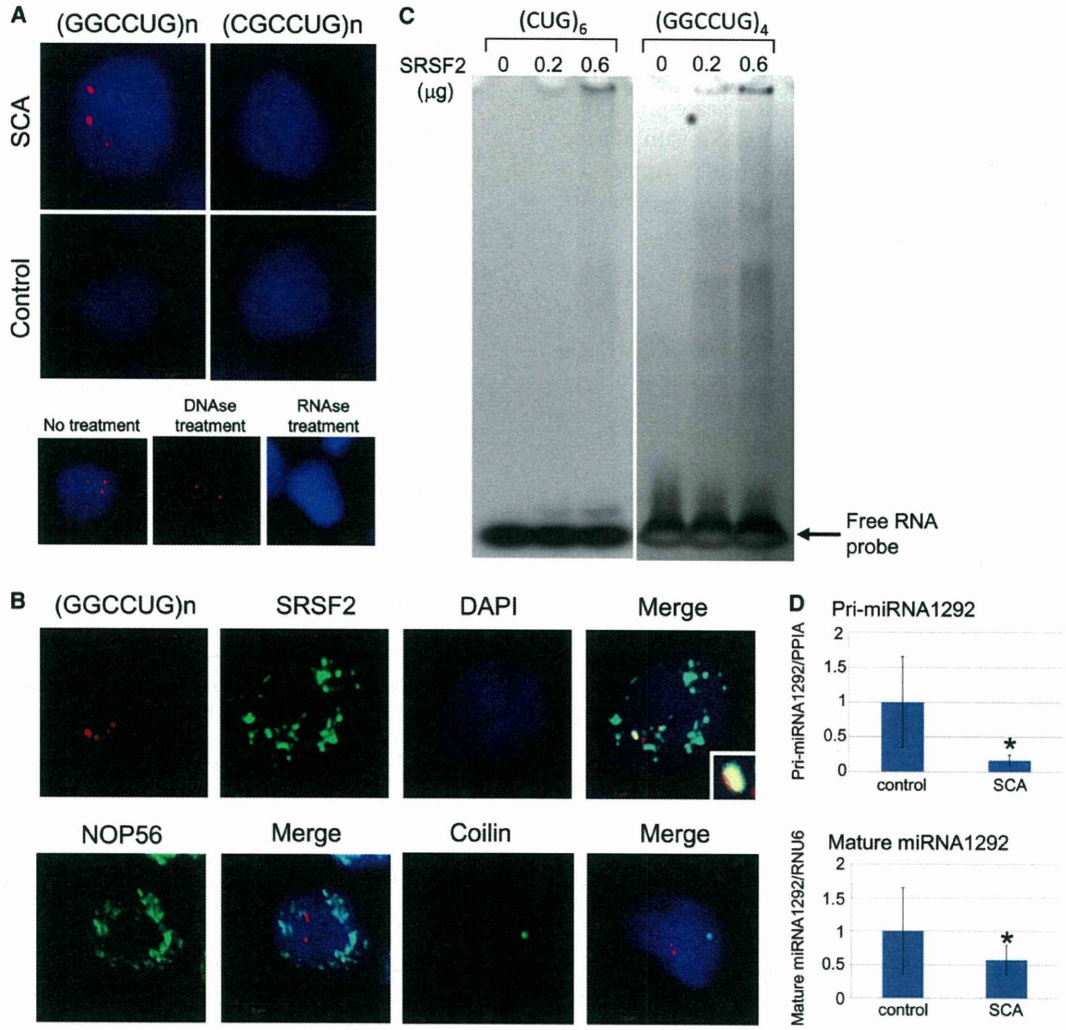

Figure 6. RNA Foci Formation and Decreased Transcription of *MIR1292*

(A) Cells were fixed on coverslips and then hybridized with solutions containing either a Cy3-labeled $C(CAGGCC)_2CAG$ or $G(CAGGCG)_2CAG$ oligonucleotide probe (1 ng/μl). For controls, the cells were treated with 1000 U/ml DNase or 100 μg/ml RNase for 1 hr at 37°C prior to hybridization, as indicated. After a wash step, coverslips were placed on the slides in the presence of ProLong Gold with DAPI mounting media (Molecular Probes, Tokyo, Japan) and photographed with a fluorescence microscope. The upper panels indicate LCLs from an SCA case and a control hybridized with $C(CAGGCC)_2CAG$ (left) or $G(CAGGCG)_2CAG$ (right). Red and blue signals represent RNA foci and the nucleus (DAPI staining), respectively. Similar RNA foci formation was confirmed in LCLs from another index case. The lower panels show RNA foci in SCA LCLs treated with DNase or RNase.

(B) Double staining was performed with the probe for $(GGCCUG)_n$ (red) and anti-SRSF2, NOP56, or coilin antibody (green).

(C) Gel-shift assays revealed specific binding of SRSF2 to $(GGCCUG)_4$ but little to $(CUG)_6$.

(D) RNA samples (10 ng) were extracted from LCLs of controls ($n = 3$) and cases ($n = 6$). MiRNAs were measured with the use of a TaqMan probe for precursor (Pri-) and mature *MIR1292*. The data indicate the mean ± SD, relative to the levels of *PPIA* or *RNU6*. *: $p < 0.05$.

on SCAs with noncoding repeat expansions. The common hallmark in these noncoding repeat expansion disorders is transcribed repeat nuclear accumulations with respective repeat RNA-binding proteins, which are considered to primarily trigger and develop the disease at the RNA level. However, multiple different mechanisms are likely to be involved in each disorder. There are at least two possible explanations for the motor neuron involvement of SCA36: gene- and tissue-specific splicing specificity of *SRSF2* and involvement of miRNA. In SCA36, there is the possibility that the adverse effect of the expansion mutation is mediated by downregulation of miRNA expression. The biochemical implication of miRNA involvement cannot be evaluated in this study, because availability of tissue samples from affected cases was limited to LCLs. Given definitive downregulation of miRNA 1292 in LCLs, we should await further study to substantiate its involvement in affected tissues. Elucidating which mechanism(s) plays a critical role in the pathogenesis will be required for determining whether cerebellar degeneration and motor neuron disease occur through a similar scenario.

In conclusion, expansion of the intronic GGCCTG hexanucleotide repeat in *NOP56* causes a unique form of SCA, SCA36, which shows not only ataxia but also motor neuron dysfunction. This characteristic disease phenotype can be explained by the combination of RNA gain of function and *MIR1292* suppression. Additional studies are required to investigate the roles of each mechanistic component in the pathogenesis of SCA36.

Supplemental Data

Supplemental Data include one figure and three tables and can be found with this article online at http://www.cell.com/AJHG/.

Acknowledgments

This work was supported mainly by grants to A.K. and partially by grants to T.M., Y.I., H.K., and K.A. We thank Norio Matsuura, Kokoro Iwasawa, and Kouji H. Harada (Kyoto University Graduate School of Medicine).

Received: February 23, 2011
Revised: May 8, 2011
Accepted: May 18, 2011
Published online: June 16, 2011

Web Resources

The URLs for data presented herein are as follows:

ESEfinder 3.0, http://rulai.cshl.edu/cgi-bin/tools/ESE3/esefinder.cgi?process=home
NCBI, http://www.ncbi.nlm.nih.gov/
Target Scan Human 5.1, http://www.targetscan.org/
UCSC Genome Bioinformatics, http://genome.ucsc.edu

References

1. Harding, A.E. (1982). The clinical features and classification of the late onset autosomal dominant cerebellar ataxias. A study of 11 families, including descendants of the 'the Drew family of Walworth'. Brain *105*, 1–28.
2. Matilla-Dueñas, A., Sánchez, I., Corral-Juan, M., Dávalos, A., Alvarez, R., and Latorre, P. (2010). Cellular and molecular pathways triggering neurodegeneration in the spinocerebellar ataxias. Cerebellum *9*, 148–166.
3. Schöls, L., Bauer, P., Schmidt, T., Schulte, T., and Riess, O. (2004). Autosomal dominant cerebellar ataxias: clinical features, genetics, and pathogenesis. Lancet Neurol. *3*, 291–304.
4. Ohta, Y., Hayashi, T., Nagai, M., Okamoto, M., Nagotani, S., Nagano, I., Ohmori, N., Takehisa, Y., Murakami, T., Shoji, M., et al. (2007). Two cases of spinocerebellar ataxia accompanied by involvement of the skeletal motor neuron system and bulbar palsy. Intern. Med. *46*, 751–755.
5. Daughters, R.S., Tuttle, D.L., Gao, W., Ikeda, Y., Moseley, M.L., Ebner, T.J., Swanson, M.S., and Ranum, L.P. (2009). RNA gain-of-function in spinocerebellar ataxia type 8. PLoS Genet. *5*, e1000600.
6. Sato, N., Amino, T., Kobayashi, K., Asakawa, S., Ishiguro, T., Tsunemi, T., Takahashi, M., Matsuura, T., Flanigan, K.M., Iwasaki, S., et al. (2009). Spinocerebellar ataxia type 31 is associated with "inserted" penta-nucleotide repeats containing (TGGAA)n. Am. J. Hum. Genet. *85*, 544–557.
7. White, M.C., Gao, R., Xu, W., Mandal, S.M., Lim, J.G., Hazra, T.K., Wakamiya, M., Edwards, S.F., Raskin, S., Teive, H.A., et al. (2010). Inactivation of hnRNP K by expanded intronic AUUCU repeat induces apoptosis via translocation of PKCdelta to mitochondria in spinocerebellar ataxia 10. PLoS Genet. *6*, e1000984.
8. Kruglyak, L., Daly, M.J., Reeve-Daly, M.P., and Lander, E.S. (1996). Parametric and nonparametric linkage analysis: a unified multipoint approach. Am. J. Hum. Genet. *58*, 1347–1363.
9. Bakalkin, G., Watanabe, H., Jezierska, J., Depoorter, C., Verschuuren-Bemelmans, C., Bazov, I., Artemenko, K.A., Yakovleva, T., Dooijes, D., Van de Warrenburg, B.P., et al. (2010). Prodynorphin mutations cause the neurodegenerative disorder spinocerebellar ataxia type 23. Am. J. Hum. Genet. *87*, 593–603.
10. Wang, J.L., Yang, X., Xia, K., Hu, Z.M., Weng, L., Jin, X., Jiang, H., Zhang, P., Shen, L., Guo, J.F., et al. (2010). TGM6 identified as a novel causative gene of spinocerebellar ataxias using exome sequencing. Brain *133*, 3510–3518.
11. Cagnoli, C., Michielotto, C., Matsuura, T., Ashizawa, T., Margolis, R.L., Holmes, S.E., Gellera, C., Migone, N., and Brusco, A. (2004). Detection of large pathogenic expansions in FRDA1, SCA10, and SCA12 genes using a simple fluorescent repeat-primed PCR assay. J. Mol. Diagn. *6*, 96–100.
12. Matsuura, T., and Ashizawa, T. (2002). Polymerase chain reaction amplification of expanded ATTCT repeat in spinocerebellar ataxia type 10. Ann. Neurol. *51*, 271–272.
13. Warner, J.P., Barron, L.H., Goudie, D., Kelly, K., Dow, D., Fitzpatrick, D.R., and Brock, D.J. (1996). A general method for the detection of large CAG repeat expansions by fluorescent PCR. J. Med. Genet. *33*, 1022–1026.
14. Hashikata, H., Liu, W., Inoue, K., Mineharu, Y., Yamada, S., Nanayakkara, S., Matsuura, N., Hitomi, T., Takagi, Y., Hashimoto, N., et al. (2010). Confirmation of an association of single-nucleotide polymorphism rs1333040 on 9p21 with familial and sporadic intracranial aneurysms in Japanese patients. Stroke *41*, 1138–1144.
15. Wahl, M.C., Will, C.L., and Lührmann, R. (2009). The spliceosome: design principles of a dynamic RNP machine. Cell *136*, 701–718.
16. Lechertier, T., Grob, A., Hernandez-Verdun, D., and Roussel, P. (2009). Fibrillarin and Nop56 interact before being co-assembled in box C/D snoRNPs. Exp. Cell Res. *315*, 928–942.
17. Liquori, C.L., Ricker, K., Moseley, M.L., Jacobsen, J.F., Kress, W., Naylor, S.L., Day, J.W., and Ranum, L.P. (2001). Myotonic dystrophy type 2 caused by a CCTG expansion in intron 1 of ZNF9. Science *293*, 864–867.
18. Taneja, K.L., McCurrach, M., Schalling, M., Housman, D., and Singer, R.H. (1995). Foci of trinucleotide repeat transcripts in nuclei of myotonic dystrophy cells and tissues. J. Cell Biol. *128*, 995–1002.
19. Winter, J., Jung, S., Keller, S., Gregory, R.I., and Diederichs, S. (2009). Many roads to maturity: microRNA biogenesis pathways and their regulation. Nat. Cell Biol. *11*, 228–234.
20. Zhao, Y., and Srivastava, D. (2007). A developmental view of microRNA function. Trends Biochem. Sci. *32*, 189–197.
21. Eacker, S.M., Dawson, T.M., and Dawson, V.L. (2009). Understanding microRNAs in neurodegeneration. Nat. Rev. Neurosci. *10*, 837–841.

22. Hébert, S.S., and De Strooper, B. (2009). Alterations of the microRNA network cause neurodegenerative disease. Trends Neurosci. *32*, 199–206.
23. Tsuzuki, K., and Ozawa, S. (2005). Glutamate Receptors. Encyclopedia of life sciences. John Wiley and Sons, Ltd., http://onlinelibrary.com/doi/10.1038/npg.els.0005056.
24. Nutini, M., Frazzini, V., Marini, C., Spalloni, A., Sensi, S.L., and Longone, P. (2011). Zinc pre-treatment enhances NMDAR-mediated excitotoxicity in cultured cortical neurons from SOD1(G93A) mouse, a model of amyotrophic lateral sclerosis. Neuropharmacology *60*, 1200–1208.
25. Sanelli, T., Ge, W., Leystra-Lantz, C., and Strong, M.J. (2007). Calcium mediated excitotoxicity in neurofilament aggregate-bearing neurons in vitro is NMDA receptor dependant. J. Neurol. Sci. *256*, 39–51.
26. Todd, P.K., and Paulson, H.L. (2010). RNA-mediated neurodegeneration in repeat expansion disorders. Ann. Neurol. *67*, 291–300.

Diabetologia (2011) 54:2247–2253
DOI 10.1007/s00125-011-2211-8

ARTICLE

Glycated albumin but not HbA_{1c} reflects glycaemic control in patients with neonatal diabetes mellitus

S. Suzuki · M. Koga · S. Amamiya · A. Nakao · K. Wada · K. Okuhara · S. Hayano · A. R. Sarhat · H. Takahashi · K. Matsuo · Y. Tanahashi · K. Fujieda

Received: 20 March 2011 / Accepted: 5 May 2011 / Published online: 5 June 2011

Abstract
Aims/hypothesis It is difficult to use HbA_{1c} as an indicator of glycaemic control in patients with neonatal diabetes mellitus (NDM) because of high levels of fetal haemoglobin (HbF) remaining in the blood. In this study, glycated albumin (GA), which is not affected by HbF, and HbA_{1c} were compared to evaluate whether they reflect glycaemic control in patients with NDM.
Methods This study included five patients with NDM. Age at diagnosis was 38±20 days. Insulin therapy was started in all patients, and levels of GA, HbA_{1c} and HbF were measured monthly for 6 months. One-month average preprandial plasma glucose (aPPG) was calculated using self-monitoring of blood glucose.
Results Plasma glucose and GA were elevated (29.7±13.1 mmol/l [n=5] and 33.3±6.9% [n=3], respectively) but HbA_{1c} was within normal limits (5.4±2.6% [35.5±4.9 mmol/mol]; n=4) at diagnosis. With diabetes treatment, aPPG (r=−0.565, p=0.002), GA (r=−0.552, p=0.003) and HbF (r=−0.855, p<0.0001) decreased with age, whereas HbA_{1c} increased (r=0.449, p=0.004). GA was strongly positively correlated with aPPG (r=0.784, p<0.0001), while HbA_{1c} showed no correlation with aPPG (r=0.221, p=0.257) and was significantly inversely correlated with HbF (r=−0.539, p=0.004).
Conclusions/interpretation GA is a useful indicator of glycaemic control in patients with NDM, whereas HbA_{1c} is influenced by age-related changes in HbF and does not accurately reflect glycaemic control.

Keywords Fetal haemoglobin · Glycated albumin · HbA_{1c} · Neonatal diabetes

Abbreviations

1,5-AG	1,5-Anhydroglucitol
aPPG	Average preprandial plasma glucose
GA	Glycated albumin
HbA	Haemoglobin A
HbF	Fetal haemoglobin
NDM	Neonatal diabetes mellitus
JDS	Japan Diabetes Society

Professor K. Fujieda, who supervised this research, died on 19 March 2010 before publication of this work.

S. Suzuki (✉) · A. R. Sarhat · H. Takahashi · K. Matsuo · Y. Tanahashi · K. Fujieda
Department of Pediatrics, Asahikawa Medical University, 2-1-1-1 Midorigaoka Higashi, Asahikawa 078-8510, Japan
e-mail: shige5p@asahikawa-med.ac.jp

M. Koga
Department of Internal Medicine, Kinki Central Hospital, Itami, Japan

S. Amamiya
Department of Pediatrics, Sapporo Tokushukai Hospital, Sapporo, Japan

A. Nakao
Department of Neonatology, Japanese Red Cross Medical Center, Tokyo, Japan

K. Wada
Department of Pediatrics, Belland General Hospital, Sakai, Japan

K. Okuhara
Department of Pediatrics, Tenshi Hospital, Sapporo, Japan

S. Hayano
Department of Pediatrics, Anjo Kosei Hospital, Anjo, Japan

NGSP	National Glycohaemoglobin Standardization Program
PH	Pancreatic hypoplasia
PNDM	Permanent NDM
pUPD6	Paternal uniparental disomy of chromosome 6
TNDM	Transient NDM

Introduction

Neonatal diabetes mellitus (NDM) is a type of diabetes that results from a single gene abnormality as a result of which insulin dependence develops within 6 months of birth [1]. NDM is clinically divided into transient NDM (TNDM), in which treatment is no longer required a few months after diagnosis, and permanent NDM (PNDM), in which lifelong treatment is required. TNDM is mainly caused by the overexpression of an imprinted region of chromosome 6q24 with paternal expression (i.e., paternal uniparental disomy of chromosome 6 [pUPD6], paternal 6q24 duplication, or methylation defect of maternal 6q24). In most cases, diabetes occurs within 1 week of birth, with remission in an average of 3 months [2, 3]. PNDM is mainly caused by an abnormality of the *KCNJ11* gene that encodes the Kir6.2 subunit of the ATP-sensitive potassium channel of pancreatic beta cells, with onset at a mean age of 7 weeks [3, 4].

Glycation of various proteins is known to occur at higher rates in individuals with diabetes compared with those without diabetes. Some of these glycated proteins are thought to be involved in the onset and progression of chronic diabetic complications [5]. Of these glycated proteins, HbA_{1c} is widely used as an indicator of glycaemic control [6]. Since the erythrocyte lifespan is approximately 120 days, HbA_{1c} levels reflect the plasma glucose levels over the preceding 2–3 months. However, HbA_{1c} levels are affected in some diseases that shorten the erythrocyte lifespan, such as haemolytic anaemia and renal anaemia, which are associated with lowered levels of HbA_{1c} [7]. Furthermore, the accuracy of some HbA_{1c} analysis methods is affected by the presence of variant haemoglobins [8]. Thus, HbA_{1c} levels may not accurately reflect glycaemic control in these situations [8]. In addition to variant haemoglobin, some assays and calculation methods for estimating HbA_{1c} indicate that HbA_{1c} levels appear low when fetal haemoglobin (HbF) levels are high [9, 10]. HbF is the main haemoglobin present during the fetal period and accounts for 80–90% of haemoglobin just after birth, whereas haemoglobin A (HbA) accounts for only 10–20% [11]. After birth, HbF is gradually replaced by HbA; by 6 months of age, most of the haemoglobin present is HbA. Therefore, if HbA_{1c}, a glycosylation product of HbA, is reported as a percentage of total haemoglobin, the influence of HbF in neonates leads to apparently low HbA_{1c}. It is therefore difficult to use HbA_{1c} as an indicator of glycaemic control in neonates. Glycation of any type of haemoglobin can be detected by affinity chromatography [12]. However, glycated haemoglobin levels appear to be low when HbF levels are high, because of the lower glycation rate of HbF compared with that of HbA [10]. Consequently, none of the current glycaemic indicators have been useful for patients with NDM; plasma glucose analysis is therefore currently used for the diagnosis and treatment of NDM.

Glycated albumin (GA) is also used as an indicator of glycaemic control [13]. Because the half-life of serum albumin is shorter than that of erythrocytes, GA reflects plasma glucose levels over a shorter period of time [14]. Thus, use of GA has been advocated for monitoring short-term changes in glycaemic control [15]. In addition, because GA is not affected by haemoglobin metabolism, it is a useful indicator of glycaemic control in patients with haemolytic anaemia [16]. Moreover, we have reported that, because GA is not affected by HbF, it can be used as an indicator of glycaemic control in neonates, when measured in umbilical cord blood [17]. Therefore, GA and HbA_{1c} were compared in this study to evaluate their utility in monitoring glycaemic control in patients with NDM.

Methods

Study patients This study included five patients with NDM (PNDM, 4; TNDM, 1) who were referred to the Department of Pediatrics, Asahikawa Medical University (Table 1). Their gestation period was 39±1.7 weeks, and their birthweight was 2,069±601 g. The birthweight SD score corrected for gestational age in Japanese babies [18], was low (−2.5±0.9 SD). Age at diagnosis was 38±20 days. Insulin therapy was started in all patients immediately after diagnosis. HbA_{1c} and GA were measured in four and three patients, respectively, at the time of diagnosis. Three patients were referred immediately to the department, and the other two patients were referred later. Age at referral was 58± 11 days. After referral, HbA_{1c}, GA and HbF were measured monthly for 6 months after diagnosis. Based on the results of self-monitoring of blood glucose (3.8±2.3 times/day) before feeding, average preprandial plasma glucose (aPPG) levels were calculated for a 1 month period.

The *KCNJ11* gene analysis was performed by direct sequencing in all patients [3]. Heterozygous mutations were identified in three patients (Patient 1, p.V59M; Patient 4, p. R201C; and Patient 5, p.F35V). Patient 2 had pancreatic hypoplasia (PH). Patient 3 exhibited TNDM and insulin therapy was discontinued at 5 months of age. We performed microsatellite marker analysis of chromosome 6 [3] on Patient 3, confirming that the patient had TNDM due to

Table 1 Characteristics of the patients with neonatal diabetes in this study

Patient	Sex	Type	Aetiology	At birth			At diagnosis					Age at enrolment (days)	Assay for HbA_{1c}
				Gestation (weeks)	BW (g)	BW (SDS)[a]	Age (days)	Plasma glucose (mmol/l)	HbA_{1c} (%)	HbA_{1c} (mmol/mol)	GA (%)		
1	Male	PNDM	*KCNJ11*	41	2,582	1.9	53	47.5	8.9	73.8	40.8	53	G8
2	Female	PNDM	PH	37	1,353	3.7	58	19.4	5.1	32.2	31.7	58	8160
3	Male	TNDM[b]	pUPD6	37	1,514	2.8	19	17.6	2.6	4.9	NA	75	G8
4	Male	PNDM	*KCNJ11*	39	2,258	2.5	14	24.8	NA	NA	NA	57	8160
5	Male	PNDM	*KCNJ11*	39	2,640	1.4	45	39.2	4.9	30.1	27.3	45	G8
Mean ± SD				39±1.7	2,069±601	2.5±0.9	38±20	29.7±13.1	5.4±2.6	35.5±4.9	33.3±6.9	58±11	

BW, birthweight; G8, Tosoh HLC-723G8; 8160, ADAMS-HA-8160; NA, not available

[a] SD score (SDS) based on the average Japanese baby with correction for gestational age [18]; [b] Remission at 5 months of age

pUPD6. All steps of this study, including DNA analysis, were approved by the Ethics Committees at Asahikawa Medical University, and the study complied with the ethical guidelines of the Helsinki Declaration as revised in 2000. All patients' parents provided written informed consent.

Laboratory methods Plasma glucose at diagnosis was determined using a standard laboratory assay. HbA_{1c} levels were determined by use of the following two methods: HPLC method using HLC-723G8 (Tosoh, Tokyo, Japan) for Patients 1, 3, and 5, and ADAMS-A1C HA-8160 (Arkray, Kyoto, Japan) for Patients 2 and 4. HbA_{1c} is calculated as a percentage of total haemoglobin. The value for HbA_{1c} (%) was estimated as a National Glycohaemoglobin Standardization Program (NGSP) equivalent value (%), calculated by the formula HbA_{1c} (%) = HbA_{1c} (Japan Diabetes Society: JDS) (%) +0.4%. This calculation takes into consideration the relationship between HbA_{1c} (JDS) (%), measured by the previous Japanese standard substance and measurement methods, and HbA_{1c} (NGSP) [19]. Normal control HbA_{1c} (NGSP) levels for adults are in the range of 4.7–6.2%.

Serum GA was determined by an enzymatic method using an albumin-specific protease, ketoamine oxidase, and an albumin assay reagent (Lucica GA-L; Asahi Kasei Pharma, Tokyo, Japan) [20]. GA was hydrolysed to amino acids by an albumin-specific proteinase and then oxidised by ketoamine oxidase, producing hydrogen peroxide, which was measured quantitatively. Serum GA levels were calculated as the percentage of GA relative to total albumin. Normal control serum GA levels for adults are in the range 11.0–16.0%. Albumin was measured in the same serum sample using a new bromocresol purple method (Lucica GA-L; Asahi Kasei Pharma). Normal control serum albumin levels for adults are in the range 39–49 g/l with this method.

Statistical analysis Results are expressed as means ± SD. Simple regression analyses were used to assess the associations between continuous variables. All analyses were performed using SPSS version 16.0 (SPSS, Chicago, IL, USA). p values were calculated and the level of significance was set at $p<0.05$.

Results

At the time of diagnosis, plasma glucose and GA were markedly elevated in our study group (29.7±13.1 mmol/l [n=5] and 33.3±6.9% [n=3], respectively) (Table 1). On the other hand, HbA_{1c} was elevated only in patient 1; it was within normal limits in patients 2 and 4 and was low in patient 3. The mean HbA_{1c} was 5.4±2.6% (35.5±4.9 mmol/mol) (n=4).

Figure 1 depicts the clinical course of patient 1 from the time of diagnosis. Patient 1, a boy born at 41 weeks of gestation weighing 2,582 g (−1.9 SD) at birth, exhibited poor feeding for several days before the first evaluation and was admitted to the local hospital at 53 days of age because he was 'not doing well'. Laboratory tests at the initial evaluation showed the following: PG, 47.5 mmol/l; GA, 40.8%; HbA_{1c}, 8.9% (73.8 mmol/mol); HbF, 22.2%; serum C-peptide level, <0.06 nmol/l; and pH, 6.826 on arterial blood gas analysis. Diabetic ketoacidosis was diagnosed, and insulin therapy was started immediately. With insulin therapy, his general condition improved and his aPPG and GA levels decreased. However, despite treatment for diabetes, HbA_{1c} levels gradually increased until 5 months of age. After that point, HbA_{1c} levels decreased. HbF levels decreased over time.

Figure 2 depicts the clinical course (in other words, the relationship between diabetes treatment and age [days]) for aPPG, GA and HbA_{1c} in all patients. aPPG was significantly inversely correlated with age as expected, given the course of treatment for diabetes (r=−0.565, p=0.002). Similarly, GA was also significantly inversely correlated with age (r=-0.552, p=0.003). On the other hand, HbA_{1c} was significantly positively correlated with age (r=0.449, p=0.004). HbF also decreased with age, but at 7 months of age (215±18 days), the value (3.2±1.3%) was still higher than normal (<2%).

Next, we evaluated whether GA or HbA_{1c} reflected glycaemic control in NDM patients. GA was strongly positively correlated with aPPG (r=0.784, p<0.0001) (Fig. 3). However, HbA_{1c} showed no correlation with aPPG (r=0.221, p=0.257), and HbA_{1c} was significantly inversely correlated with HbF (r=−0.539, p=0.004) (Fig. 3).

Discussion

At the time of diagnosis, the mean HbA_{1c} was within normal limits for all patients with NDM. In the neonatal

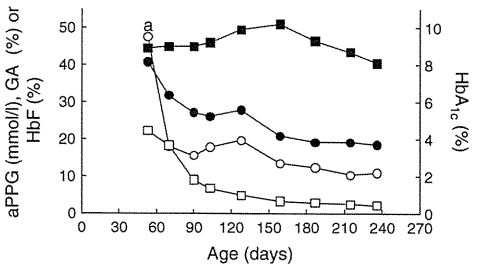

Fig. 1 Clinical course of Patient 1. The time courses of aPPG (white circles), GA (black circles), HbA_{1c} (black squares), and HbF (white squares) since diagnosis of diabetes in Patient 1 are shown. [a]Plasma glucose at diagnosis. To convert values for HbA_{1c} in % to mmol/mmol, subtract 2.15 and then multiply by 10.929